Euro. Jnl of Applied Mathematics (2013), *vol.* 24, *pp.* 161–177.
doi:10.1017/S0956792512000344

A model for the evolution of the thermal bar system

DUNCAN E. FARROW

Mathematics & Statistics, Murdoch University, Murdoch, Perth WA 6150, Australia
email: D.Farrow@murdoch.edu.au

(*Received 8 December 2011; revised 17 September 2012; accepted 18 September 2012; first published online 30 October 2012*)

A new framework for modelling the evolution of the thermal bar system in a lake is presented. The model assumes that the thermal bar is located between two regions: the deeper region, where spring warming leads to overturning of the entire water column, and the near shore shallower region, where a stable surface layer is established. In this model the thermal bar moves out slightly more quickly than predicted by a simple thermal balance. Also, the horizontal extent of the thermal bar region increases as it moves out from the shore.

Key words: Thermal bar, convection, lakes

1 Introduction

At the end of winter, the temperature of the water in many temperate lakes is less than $T_m = 4°\text{C}$, the temperature at which fresh water achieves its maximum density. As spring progresses and the water is warmed, the near-shore shallow waters heat more rapidly than the deeper parts. As a consequence, the 4°C isotherm propagates out from the shore, and different conditions prevail to either side of it. In the deeper regions the heating leads to a destabilising of the water column and active mixing. In the shallows where the water is warmer than 4°C, the heating leads to a stable stratification. The boundary between these two regions is called the thermal bar. In the intermediate depths there is a stably stratified layer near the surface and active convection at depth where the water is cooler than 4°C. The general horizontal temperature gradient also induces a double-celled circulation pattern with downwelling in the vicinity of the thermal bar. A similar phenomenon occurs at the end of autumn as the lake is cooled towards 4°C. The shallow waters cool more rapidly, and because of the symmetry of the density relation about 4°C, a system similar to the one that occurs during spring warming develops.

Previous modelling of the thermal bar system has fallen into two broad categories. The first category has concentrated on the propagation of the thermal bar by considering in detail the heat transfer in the system. Elliott and Elliott [9] modelled the propagation of the thermal bar by distributing the surface heat flux over the local depth. For constant bottom slope case this leads to the thermal bar moving out from the shore at a constant

speed given by

$$\text{Propagation speed} = \frac{I_0}{\rho_0 C_p A \Delta T_0}, \tag{1.1}$$

where I_0 is the surface heat flux, ρ_0 is the reference density, C_p is the specific heat, A is the bottom slope and $\Delta T_0 = T_m - T_0$, where T_0 is the initial temperature of the lake. Using Lake Ladoga as an example [19] gives $I_0 \sim 200$ Wm^{-2}, $A \sim 10^{-3}$, and the usual values for the other parameters give a propagation speed of the order of 2 km per day. This means that the thermal bar can persist for several weeks in large lakes such as Lake Ladoga [19]. Most previous studies of the propagation the thermal bar have investigated experimentally observed departures [6, 17] from (1.1). Zilitinkevich *et al.* [21] generalised the work of [9] to include significant horizontal heat transfer in the vicinity of the thermal bar. This additional heat transfer leads to the thermal bar propagating more quickly than (1.1). The analysis in [21] has been generalised to circular lakes in [22].

The second category has focussed on the general circulation associated with the thermal bar system. These include the quasi-steady state model of Elliott [8], the steady state models that included Coriolis effects of Csanady [5] and Huang [16] and the asymptotic unsteady results of Farrow [10, 12]. Unsteady asymptotic results that include Coriolis effects where found by Farrow and McDonald [13]. Besides elucidating the general circulation features of the thermal bar system, the models show how inertia and advection can lead to the thermal bar propagating out from the shore either more slowly or more quickly than the speed given in (1.1), especially for lakes with bottom slopes greater than $\sim 10^{-2}$ [11, 18]. These results have gone some way to explaining the 'two-speed' propagation of the thermal bar observed experimentally [17].

In this paper a different approach is used to model the evolution of the thermal bar system. The framework for the model is that the position of the thermal bar is at the boundary between the stably stratified shallow region and the deeper unstable region. Thus, the model focuses on the stability of the local water column rather than considering the lake system as a whole and ignores any horizontal transfer of heat or momentum. This approach is justified so long as horizontal transport of heat and momentum is negligible, which is the case for lakes with small bottom slopes and where there are no other significant drivers of horizontal mixing (such as wind). The results of this work are less applicable to laboratory experiments which usually have bottom slopes of $\sim 10^{-1}$ so that horizontal transport cannot be ignored, at least for larger times.

In Section 2 a model for the thermal bar system, including the heating mechanism and some solutions, are found for the small bottom slope limit. In Section 3 the solutions from Section 2 are subjected to a linear stability analysis. In that analysis it is assumed that horizontal processes can be ignored. The stability problem is analysed in two ways. The first is in the zero critical wavenumber limit, and then subsequently numerically for general critical wavenumber. The results are then discussed in Section 4 in the context of the propagation of the thermal bar.

2 Model formulation

The thermal bar system is modelled by the natural convection of a fluid contained in the semi-infinite two-dimensional triangular domain bounded by the lines $\tilde{z} = 0$ and $\tilde{z} = -A\tilde{x}$

https://doi.org/10.1017/S0956792512000344 Published online by Cambridge University Press

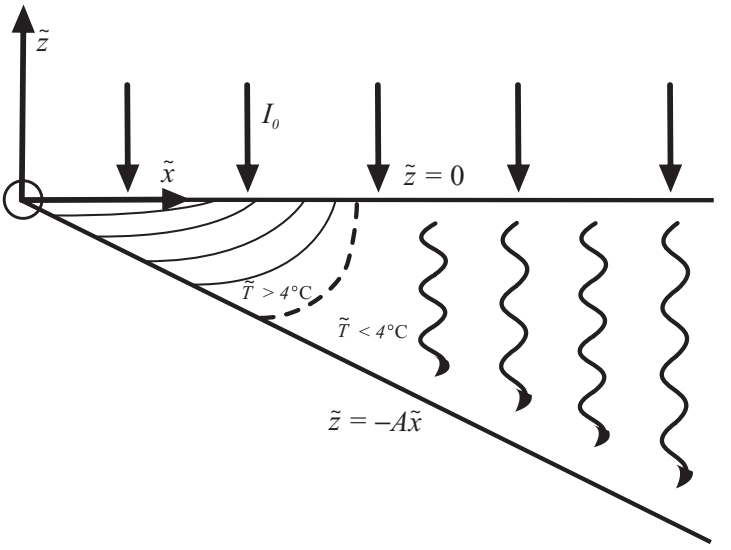

FIGURE 1. Schematic of flow domain showing conceptual flow structure of thermal bar system.

in the $(\tilde{x}, \tilde{z})$-plane where A is the bottom slope. The flow domain and coordinate system are shown in Figure 1. The flow is driven by a surface heat flux of (constant) magnitude $I_0 \mathrm{Wm}^{-2}$. The precise mechanism whereby the heat enters the system is specified below.

An important part of the thermal bar phenomenon is the local density maximum of fresh water at 4°C. For temperatures near 4°C, the density/temperature relationship is well approximated by

$$\rho = \rho_m(1 - \beta(\tilde{T} - T_m)^2), \tag{2.1}$$

where ρ_m is the maximum density at the maximum density temperature T_m and $\beta \approx 6.8 \times 10^{-6}\,{}^\circ\mathrm{C}^{-2}$. This quadratic dependence provides reasonable accuracy over the temperature range 0°–8°C and is used by many workers modelling flows near the density maximum.

Assuming that temperature differences are sufficiently small that the Boussinesq approximation is appropriate, the equations of motion are

$$\frac{D\tilde{u}}{D\tilde{t}} = -\frac{1}{\rho_m}\tilde{p}_{\tilde{x}} + \nu\nabla^2\tilde{u}, \tag{2.2a}$$

$$\frac{D\tilde{w}}{D\tilde{t}} = -\frac{1}{\rho_m}\tilde{p}_{\tilde{z}} + \nu\nabla^2\tilde{w} + g\beta(\tilde{T} - T_m)^2, \tag{2.2b}$$

$$\frac{D\tilde{T}}{D\tilde{t}} = \kappa\nabla^2\tilde{T} + Q(\tilde{x}, \tilde{z}, \tilde{t}), \tag{2.2c}$$

$$\tilde{u}_{\tilde{x}} + \tilde{w}_{\tilde{z}} = 0, \tag{2.2d}$$

where $\tilde{u}$ and $\tilde{w}$ are the horizontal and vertical velocities respectively, $\tilde{T}$ is the temperature, $\tilde{p}$ is the pressure perturbation, Q is the volumetric heating rate (discussed below), ν is the kinematic viscosity, κ is the thermal diffusivity, $D/D\tilde{t} = \partial/\partial\tilde{t} + \tilde{u}\partial/\partial\tilde{x} + \tilde{w}\partial/\partial\tilde{z}$ is the material derivative, $\nabla^2 = \partial^2/\partial\tilde{x}^2 + \partial^2/\partial\tilde{z}^2$ is the two-dimensional Laplacian and dependent variable subscripts denote differentiation.

https://doi.org/10.1017/S0956792512000344 Published online by Cambridge University Press

The system is driven by the internal heating term Q in (2.2c). In both nature and laboratory models of the thermal bar, the main heating mechanism is via the absorption of light from either the sun or artificial lamps. As light at a particular wavelength is absorbed with depth, its intensity drops exponentially with depth according to Beer's law,

$$I(\tilde{z}) = I_0 \exp(\tilde{\eta}\tilde{z}), \tag{2.3}$$

where $\tilde{\eta}\mathrm{m}^{-1}$ is the attenuation coefficient. The attenuation coefficient $\tilde{\eta}$ depends on the wavelength of the light and the turbidity of the water. In modelling flows driven by the absorption of light from the sun or lamps, the overall intensity is often distributed between three or four discrete wavelengths each with their own attenuation coefficient [2, 3]. For simplicity, it is assumed in the present work that the light incident at the surface can be characterised by a single attenuation coefficient. Under this assumption, the volumetric heating term Q in (2.2c) is given by

$$Q = \frac{I_0\tilde{\eta}}{\rho_m C_p} \exp(\tilde{\eta}\tilde{z}), \tag{2.4}$$

where C_p is the specific heat of water. Note the the thermal bar in natural lakes is a response to gradual seasonal changes in the thermal forcing. This means that the step change implicit in (2.4) is an approximation of the thermal forcing. The effect of gradual heating on the circulation structure of the thermal bar was investigated by Farrow [12]. In the present work where the 'frozen time' assumption is made, the temporal evolution of the thermal forcing has little impact on the results.

To complete the model, boundary and initial conditions need to be specified. For $\tilde{u}$ and $\tilde{w}$, it is assumed that the surface $\tilde{z} = 0$ is stress-free and remains flat, thus

$$\tilde{u}_{\tilde{z}} = 0 \quad \text{and} \quad \tilde{w} = 0 \quad \text{on} \quad \tilde{z} = 0. \tag{2.5}$$

The bottom $\tilde{z} = -A\tilde{x}$ is assumed to be non-slip so

$$\tilde{u} = \tilde{w} = 0 \quad \text{on} \quad \tilde{z} = -A\tilde{x}. \tag{2.6}$$

For the temperature, it is supposed that all the heat input and output is accounted for by the internal heating term Q in (2.2c). In fact, since the flow domain is of finite depth, there will be some light that penetrates to the bottom of the flow domain. In the shallows near the shore $\tilde{x} = 0$, most of the light will reach the bottom. For the purposes of the current work, it is assumed that this excess light passes through the bottom of the flow domain and disappears. In their related work on solar-induced natural convection near lake boundaries, Farrow and Patterson [14] assumed that the excess radiation was absorbed by the bottom and then the associated heat was re-emitted as a boundary heat flux. This introduces another possible source for instability in a region which is not the focus of the present work, so the excess heat is ignored. Under these assumptions, the top and bottom boundary conditions on the temperature are

$$\tilde{T}_{\tilde{z}} = 0 \quad \text{on} \quad \tilde{z} = 0 \quad \text{and} \quad A\tilde{T}_{\tilde{x}} + \tilde{T}_{\tilde{z}} = 0 \quad \text{on} \quad \tilde{z} = -A\tilde{x}. \tag{2.7}$$

https://doi.org/10.1017/S0956792512000344 Published online by Cambridge University Press

The initial conditions for this model are $\tilde{u} = \tilde{w} = 0$ and $\tilde{T} = T_0 < T_m$ at $\tilde{t} = 0$, that is the fluid is at rest and is at a uniform temperature less than the temperature of maximum density.

The system of equations are non-dimensionalised following the scheme used by Farrow [10]. There is no length scale associated with the geometry of the flow domain. Suppose that the surface heat flux I_0 is distributed uniformly over the local depth, then balancing this against the unsteady term in (2.2c) yields a scale for $\tilde{T} - T_0$

$$\tilde{T} - T_0 \sim I_0 t/(\rho_m C_p A \tilde{x}). \tag{2.8}$$

The position at which $\tilde{T} = T_m$, the maximum density temperature, is

$$\tilde{x}_m \sim I_0 \tilde{t}/(\Delta T_0 \rho_m C_p A) \tag{2.9}$$

where $\Delta T_0 = T_m - T_0$ and the local depth will be $h_m \sim A\tilde{x}_m$. This argument is identical to that in Section 1 which led to (1.1). Viscous effects will be felt over a depth h_m in a time scale of $\tau = h_m^2/\nu$. Identifying $\tilde{t}$ with τ yields time and length scales for this model,

$$\tilde{x} \sim l = \nu \Delta T_0 \rho_0 C_p/(A I_0), \tag{2.10a}$$

$$\tilde{z} \sim h = \nu \Delta T_0 \rho_0 C_p / I_0, \tag{2.10b}$$

$$\tilde{t} \sim \tau = \nu \left(\Delta T_0 \rho_0 C_p / I_0\right)^2. \tag{2.10c}$$

The temperature scale used here is $\tilde{T} - T_0 \sim \Delta T_0$. Balancing the buoyancy and pressure gradient terms in (2.2b) yields a scale for the pressure perturbation $\tilde{p} \sim \Delta \rho_0 g h$, where $\Delta \rho_0 = \rho_m \beta \Delta T_0^2$. Substitution into (2.2a) and assuming a viscous/pressure gradient balance yields a horizontal velocity scale,

$$\tilde{u} \sim U = \frac{ARa}{\sigma} \frac{h}{\tau}, \tag{2.11}$$

where $\sigma = \nu/\kappa$ is the Prandtl number and Ra is the Rayleigh number given by

$$Ra = \frac{g \Delta \rho_0 h^3}{\rho_m \nu \kappa}. \tag{2.12}$$

Finally, the continuity equation yields $\tilde{w} \sim AU$.

The system of equations (2.2a)–(2.2d) is non-dimensionalised using

$$\tilde{x} = lx,\ \tilde{z} = hz,\ \tilde{t} = \tau t,\ \tilde{u} = Uu,\ \tilde{w} = AUw,\ \tilde{p} = \Delta \rho_0 g h p \text{ and } \tilde{T} = T_0 + \Delta T_0 T, \tag{2.13}$$

where variables without a tilde are dimensionless. The dimensionless equations are

$$u_t + A^2 Ra(uu_x + wu_z)/\sigma = -p_x + A^2 u_{xx} + u_{zz}, \tag{2.14a}$$

$$w_t + A^2 Ra(uw_x + ww_z)/\sigma = -p_z/A^2 + A^2 w_{xx} + w_{zz} + (1 - T)^2/A^2, \tag{2.14b}$$

$$T_t + A^2 Ra(uT_x + wT_z)/\sigma = (A^2 T_{xx} + T_{zz})/\sigma + \eta e^{\eta z}, \tag{2.14c}$$

$$u_x + w_z = 0, \tag{2.14d}$$

https://doi.org/10.1017/S0956792512000344 Published online by Cambridge University Press

where $\eta = h\tilde{\eta}$ is the dimensionless attenuation coefficient and all variables are now non-dimensional. The domain boundaries are $z = 0$ and $z = -x$ at which the boundary conditions are

$$u_z = w = T_z = 0 \quad \text{on} \quad z = 0, \tag{2.15a}$$

$$u = w = A^2 T_x + T_z = 0 \quad \text{on} \quad z = -x. \tag{2.15b}$$

The initial conditions are $u = w = T = 0$ at $t = 0$.

The system of equations (2.14a)–(2.15b) do not admit a general analytic solution. However, the parameter A is generally small (typically 10^{-2} or less in lakes) and this can be exploited to obtain an asymptotic solution as $A \to 0$ (see, for example [4] or [10]). Letting $A \to 0$ yields a system of equations for the $O(A^0)$ solution (denoted by superscripts (0)),

$$u_t^{(0)} = -p_x^{(0)} + u_{zz}^{(0)}, \tag{2.16a}$$

$$0 = -p_z^{(0)} + (1 - T^{(0)})^2, \tag{2.16b}$$

$$T_t^{(0)} = T_{zz}^{(0)}/\sigma + \eta e^{\eta z}, \tag{2.16c}$$

$$u_x^{(0)} + w_z^{(0)} = 0, \tag{2.16d}$$

with the boundary conditions

$$u_z^{(0)} = w^{(0)} = T_z^{(0)} = 0 \quad \text{on} \quad z = 0, \tag{2.17a}$$

$$u^{(0)} = w^{(0)} = T_z^{(0)} = 0 \quad \text{on} \quad z = -x, \tag{2.17b}$$

and the initial conditions $u^{(0)} = w^{(0)} = T^{(0)} = 0$ at $t = 0$.

The zero-order temperature $T^{(0)}$ can be determined independently and is the solution of a straightforward one-dimensional conduction problem. The solution is

$$\begin{aligned} T^{(0)}(x,z,t) = \frac{t}{x}(1 - e^{-\eta x}) + \sigma \Bigg[z - e^{\eta z}/\eta + \frac{z^2}{2x}(1 - e^{-\eta x}) \\ + \frac{1}{\eta^2 x}(1 - e^{-\eta x}) + \frac{x}{6}(2 + e^{-\eta x}) \Bigg] \\ - \frac{2\sigma}{x} \sum_{n=1}^{\infty} \left(\frac{x}{n\pi}\right)^2 \eta^2 \frac{1 - (-1)^n e^{-\eta x}}{\eta^2 + (n\pi/x)^2} \exp\left(-\left(\frac{n\pi}{x}\right)^2 \frac{t}{\sigma}\right) \cos\left(\frac{n\pi z}{x}\right). \end{aligned} \tag{2.18}$$

Figure 2 shows a few profiles of $T^{(0)}$ at $x = 3$ for various times as well as the corresponding density profile. As time progresses, there is a change from a monotonic and unstable density profile to a two-layer profile with a stable layer near the surface. This transition occurs as the surface temperature $T^{(0)}(0)$ becomes larger than one. As time progresses, the depth of the stable layer increases until the temperature at the base of the water column reaches one (not shown in the figure), at which time the density profile will become stable over the entire depth.

https://doi.org/10.1017/S0956792512000344 Published online by Cambridge University Press

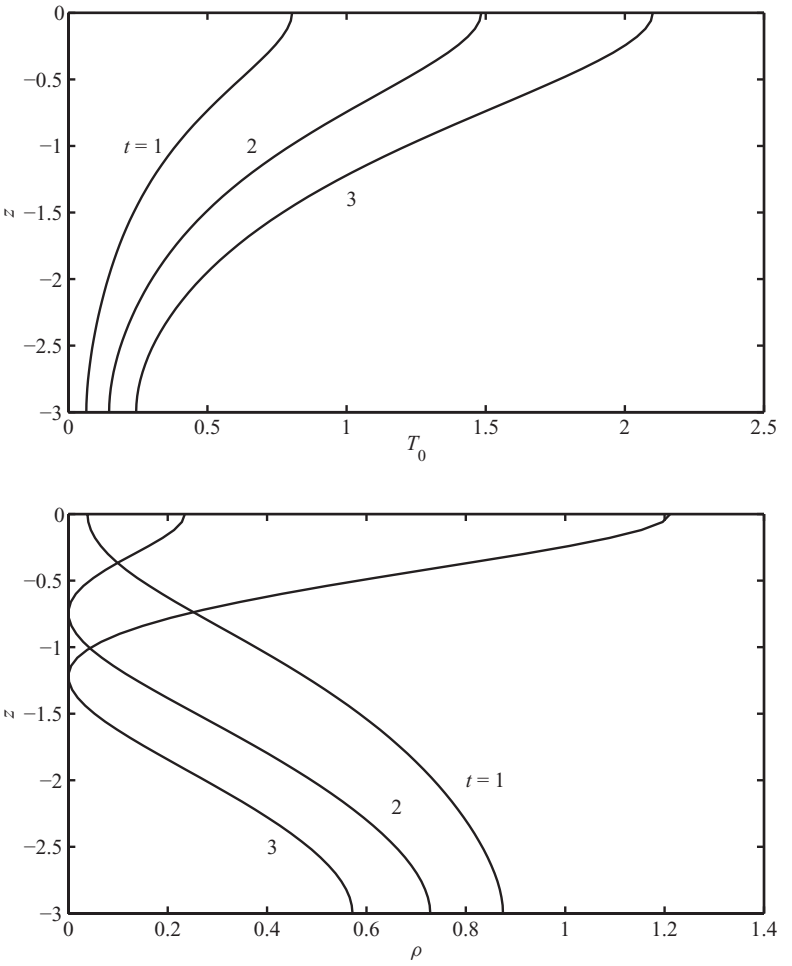

FIGURE 2. Vertical profiles of (a) $T^{(0)}$, and (b) density at $x = 3$ for various times showing transition from single layer to two-layer density structure.

The boundary value problem for $u^{(0)}$ is , despite being linear, difficult to solve as it involves the forcing term $(1 - T^{(0)})^2$, where $T^{(0)}$ is an infinite series. Fortunately, the stability problem discussed in the next section is independent of $u^{(0)}$, so no attempt is made to find $u^{(0)}$.

3 The stability problem

3.1 Formulation

The $A \to 0$ solution described in the previous section includes regions where there is less dense fluid overlying more dense fluid. This section investigates the stability of the $A \to 0$ solution using a linear stability analysis.

https://doi.org/10.1017/S0956792512000344 Published online by Cambridge University Press

The $A \to 0$ solution is perturbed in the following way:

$$u = u^{(0)} + \frac{\varepsilon}{A} U(\xi, z, t), \tag{3.1a}$$

$$w = w^{(0)} + \frac{\varepsilon}{A^2} W(\xi, z, t), \tag{3.1b}$$

$$p = p^{(0)} + \varepsilon P(\xi, z, t), \tag{3.1c}$$

$$T = T^{(0)} + \varepsilon \Theta(\xi, z, t), \tag{3.1d}$$

where $\varepsilon \ll 1$ is the perturbation parameter and $\xi = x/A$ is a rescaled horizontal coordinate. The perturbation quantities are taken to scale independent of A. In the non-dimensionalisation outlined in Section 2, A appears explicitly in the scales for x, u and w. Thus, for the perturbation velocities U and W to be $O(1)$ with respect to A, A^{-1} and A^{-2} must appear in the factors multiplying the perturbation velocities. Similarly, the horizontal scale of the perturbations need not scale with A^{-1}, thus the horizontal coordinate is rescaled.

Substitution of the perturbed quantities into (2.14a)–(2.14d), linearising with respect to A and ε and making use of (2.16a)–(2.16d) yield evolution equations for the perturbation quantities,

$$U_t = -P_\xi + U_{\xi\xi} + U_{zz}, \tag{3.2a}$$

$$W_t = -P_z + W_{\xi\xi} + W_{zz} - 2\Theta(1 - T^{(0)}), \tag{3.2b}$$

$$\sigma \Theta_t + Ra W T_z^{(0)} = (\Theta_{\xi\xi} + \Theta_{zz}), \tag{3.2c}$$

$$U_\xi + W_z = 0. \tag{3.2d}$$

Note that $u^{(0)}$ does not appear in the evolution equations. This is not surprising, as it was shown in Section 2 that the dimensional velocity u for the base flow scaled with the A. Thus, for $u^{(0)}$ to appear in the stability problem, A must also appear as a parameter. The $A \to 0$ asymptotics have explicitly excluded A as a parameter, thus $u^{(0)}$ does not appear in the stability problem. The boundary conditions on the perturbation quantities are

$$U_z = W = \Theta_z = 0 \quad \text{on} \quad z = 0 \quad \text{and} \quad U = W = \Theta_z = 0 \quad \text{on} \quad z = -x. \tag{3.3}$$

Introducing a streamfunction Ψ with $U = -\Psi_z$ and $W = \Psi_\xi$ and eliminating P from (3.2a)–(3.2d) yields

$$(\partial^2/\partial\xi^2 + \partial^2/\partial z^2)\Psi_t = (\partial^2/\partial\xi^2 + \partial^2/\partial z^2)^2 \Psi - 2\Theta_\xi(1 - T^{(0)}), \tag{3.4a}$$

$$\sigma \Theta_t + Ra \Psi_\xi T_z^{(0)} = (\partial^2/\partial\xi^2 + \partial^2/\partial z^2)\Theta. \tag{3.4b}$$

The remainder of the stability analysis makes the 'frozen time' assumption with respect to the background temperature structure. It is assumed that the background temperature is steady with respect to the evolution of the perturbation quantities. The validity of this assumption was examined by Gresho and Sani [15], who found that the frozen time assumption is justified for a linear stability analysis so long as the background temperature structure is free of step changes, which is the case here.

https://doi.org/10.1017/S0956792512000344 Published online by Cambridge University Press

The perturbation quantities are now assumed to take the particular form

$$\Psi = \mathbb{R}\{ik\psi(z)e^{st+ik\xi}\}, \tag{3.5a}$$

$$\Theta = \mathbb{R}\{\theta(z)e^{st+ik\xi}\}, \tag{3.5b}$$

where s is the instantaneous growth rate, k is the wavenumber of the disturbance and i is the imaginary unit. Substitution into (3.4a) and (3.4b) yields

$$(D^2 - k^2 - s)(D^2 - k^2)\psi = 2\theta(1 - T^{(0)}), \tag{3.6a}$$

$$(D^2 - k^2 - \sigma s)\theta = -Ra_c(x,t)k^2\psi DT^{(0)}, \tag{3.6b}$$

where the short-hand $D \equiv d/dz$ has been introduced. The boundary conditions on ψ and θ are

$$D\theta = \psi = D^2\psi = 0 \quad \text{on} \quad z = 0, \tag{3.7a}$$

$$D\theta = \psi = D\psi = 0 \quad \text{on} \quad z = -x. \tag{3.7b}$$

Specifying particular values for k and s, (3.6a) and (3.6b) along with the associated boundary conditions constitute an eigenvalue problem for $Ra_c(x,t)$, where, as implied by the notation, the value will depend on x and t which serve to specify the local conditions. The focus in this paper is on the boundary between the stable ($s < 0$) and unstable ($s > 0$) regions. Thus, the growth rate s is set to zero and the remainder of the stability analysis concentrates on the marginally stable case. The problem is now one of finding the smallest positive eigenvalue Ra_c over all possible wavenumbers. This eigenvalue (called Ra_c) is the critical Rayleigh number below which localised disturbances are damped.

3.2 Solution for $k \to 0$

Unfortunately, terms appear in (3.6a) and (3.6b), where the unknown eigenfunctions ψ and θ are multiplied by $T^{(0)}$ and $DT^{(0)}$ which are complicated functions of z. This makes a general solution of the eigenvalue problem difficult. However, Chapman and Proctor [1] have shown that for the case where the background vertical density gradient is constant and with insulated boundary conditions like those that apply here, the critical wave-number k_c at which Ra_c occurs is $k_c = 0$. Even though in the current case where the density gradient is not linear, this property can be exploited to find an expression for Ra_c analytically, at least for part of the domain.

Following Roberts [20], ψ, θ and Ra_c are expanded according to

$$\psi = \psi_0 + k^2\psi_2 + \cdots, \tag{3.8a}$$

$$\theta = \theta_0 + k^2\theta_2 + \cdots, \tag{3.8b}$$

$$Ra_c = Ra_{c0} + k^2 Ra_{c2} + \cdots, \tag{3.8c}$$

https://doi.org/10.1017/S0956792512000344 Published online by Cambridge University Press

where the symmetry of the problem has been used to eliminate odd powers of k. Substitution into (3.6a) and (3.6b) and taking the lowest order in k yields

$$D^4\psi_0 = 2\theta_0(1 - T^{(0)}), \tag{3.9a}$$

$$D^2\theta_0 = 0, \tag{3.9b}$$

for which the solution is $\theta_0 = 1$ and

$$\begin{aligned} u_0 = -D\psi_0 = &\left[\frac{t}{x}\left(1 - e^{-\eta x}\right) - 1 + \sigma\left[\frac{1}{\eta^2 x}\left(1 - e^{-\eta x}\right) + \frac{x}{6}\left(2 + e^{-\eta x}\right)\right]\right] \\ &\times\left(\frac{-z^3}{3} - \frac{3z^2x}{8} + \frac{x^3}{24}\right) - \sigma\left(\frac{z^4}{12} - \frac{z^2x^2}{10} + \frac{x^4}{60}\right) \\ &- \frac{\sigma}{2x}\left(1 - e^{-\eta x}\right)\left(\frac{z^5}{30} + \frac{z^2x^3}{24} - \frac{x^5}{120}\right) \\ &- 2\sigma\left[\frac{z}{\eta^3} - \frac{1}{\eta^4}e^{\eta z} + \frac{3z^2}{4\eta^5x^3}\left[2\eta x e^{-\eta x} - 2\left(1 - e^{-\eta x}\right) + \eta^2x^2\right]\right. \\ &\left. - \frac{1}{4\eta^5 x}\left[2\eta x e^{-\eta x} - 6\left(1 - e^{-\eta x}\right) - \eta^2x^2\right]\right] \\ &- \frac{4\sigma\eta^2}{x}\sum_{n=1}^{\infty}\left(\frac{x}{n\pi}\right)^2\frac{1 - (-1)^n e^{-\eta x}}{\eta^2 + (n\pi/x)^2}\exp\left(-\left(\frac{n\pi}{x}\right)^2\frac{t}{\sigma}\right) \\ &\times\left[\left(\frac{x}{n\pi}\right)^3\sin\left(\frac{n\pi}{x}z\right) - z\left(\frac{x}{n\pi}\right)^2\right. \\ &\left. - \frac{1}{4}\left(\frac{x}{n\pi}\right)^4\left[\left(\frac{3z^2}{x^3} + \frac{1}{x}\right)n^2\pi^2 + \left(\frac{6z^2}{x^3} - \frac{6}{x}\right)(1 - (-1)^n)\right]\right]. \end{aligned} \tag{3.10}$$

A solvability condition at the next order in k yields Ra_{c0},

$$Ra_{c0} = \left(\frac{1}{x}\int_{-x}^{0} u_0 T^{(0)} dz\right)^{-1}. \tag{3.11}$$

The above expression is apparently difficult to calculate as it involves integrating the product of two infinite series. However, by using (3.9a) and $\theta_0 = 1$, it can be shown that

$$\int_{-x}^{0} u_0 T^{(0)} dz = \int_{-x}^{0} u_0\left(1 + \frac{1}{2}D^3u_0\right) dz. \tag{3.12}$$

There is no contribution to the integral from the first term by virtue of conservation of mass. The contribution from the second term is readily calculated since it is in the form of an exact differential. Thus, when the boundary conditions (3.7a) and (3.7b) have been used, Ra_{c0} can be written as

$$Ra_{c0} = \left[\frac{1}{2x}\left(u_0D^2u_0|_{z=0} - \frac{1}{2}(Du_0)^2|_{z=-x}\right)\right]^{-1}. \tag{3.13}$$

As will be seen later, the results of this section are relevant in the deeper parts of the flow domain where the stable surface later is shallow compared with the local depth. In the

https://doi.org/10.1017/S0956792512000344 Published online by Cambridge University Press

thermal bar region the stable surface layer is deeper leading to the unstable region being physically isolated from the heat flux surface boundary condition. Under these conditions the $k_c = 0$ assumption is no longer valid. Investigating the stability characteristics of the thermal bar region requires solving (3.6a)–(3.7b) for $k_c > 0$ which motivates the numerical approach of the next section.

3.3 Numerical solution

The stability problem (3.6a)–(3.7b) is solved numerically using a shooting method similar to that described in [7]. First, a vector function $\mathbf{Y} = (\psi, D\psi, D^2\psi, D^3\psi, \theta, D\theta)^T$ is introduced so that equations (3.6a) and (3.6b) can be written in matrix form as

$$D\mathbf{Y} = K\mathbf{Y} \tag{3.14}$$

where

$$K = \begin{pmatrix} 0 & 1 & 0 & 0 & 0 & 0 \\ 0 & 0 & 1 & 0 & 0 & 0 \\ 0 & 0 & 0 & 1 & 0 & 0 \\ -k^4 & 0 & 2k^2 & 0 & 2(1 - T^{(0)}) & 0 \\ 0 & 0 & 0 & 0 & 0 & 1 \\ -Ra_c k^2 DT^{(0)} & 0 & 0 & 0 & k^2 & 0 \end{pmatrix}. \tag{3.15}$$

For fixed x and t, (3.14) is integrated from $z = -x$ to $z = 0$ using the MATLAB routine `ode45` for three different initial conditions $\mathbf{Y}(-x) = (0,0,1,0,0,0)^T$, $\mathbf{Y}(-x) = (0,0,0,1,0,0)^T$ and $\mathbf{Y}(-x) = (0,0,0,0,1,0)^T$. These three different solutions are labelled as $\mathbf{Y}_1$, $\mathbf{Y}_2$ and $\mathbf{Y}_3$ respectively and these all satisfy the boundary conditions at $z = -x$. The general solution for $\mathbf{Y}$ that satisfies all the boundary conditions at $z = 0$ will then be a linear combination of $\mathbf{Y}_1$, $\mathbf{Y}_2$ and $\mathbf{Y}_3$: $\mathbf{Y} = \alpha_1\mathbf{Y}_1 + \alpha_2\mathbf{Y}_2 + \alpha_3\mathbf{Y}_3$ for constants α_1, α_2 and α_3. The solution $\mathbf{Y}$ must satisfy the boundary conditions at $z = 0$, which can be written as

$$\begin{pmatrix} \psi_1(0) & \psi_2(0) & \psi_3(0) \\ D^2\psi_1(0) & D^2\psi_2(0) & D^2\psi_3(0) \\ D\theta_1(0) & D\theta_2(0) & D\theta_3(0) \end{pmatrix} \begin{pmatrix} \alpha_1 \\ \alpha_2 \\ \alpha_3 \end{pmatrix} = \begin{pmatrix} 0 \\ 0 \\ 0 \end{pmatrix}. \tag{3.16}$$

The only solution will be $\alpha_1 = \alpha_2 = \alpha_3 = 0$ unless the coefficient matrix in (3.16) is singular. This forms the basis of the method: searching for combinations of Ra_c and k so that the determinant of this coefficient matrix is zero.

For a fixed temperature profile $T_0(z,t)$ the aim is to find the lowest critical Rayleigh number Ra_c and corresponding critical wavenumber k_c that makes the determinant of the coefficient matrix in (3.16) zero. The numerical procedure uses the MATLAB function `fminbnd` to minimise over k a function that finds Ra_c so that the determinant of the coefficient matrix in (3.16) is zero for fixed k. This function first steps up from $Ra_c = 0$ until a zero is bracketed. The function then uses the MATLAB routine `fzero` to locate Ra_c for a particular k. A side product of the procedure is the eigenfunction associated with each Ra_c and k_c pair. This can be used to characterise the secondary motion as single- or double-celled convection.

https://doi.org/10.1017/S0956792512000344 Published online by Cambridge University Press

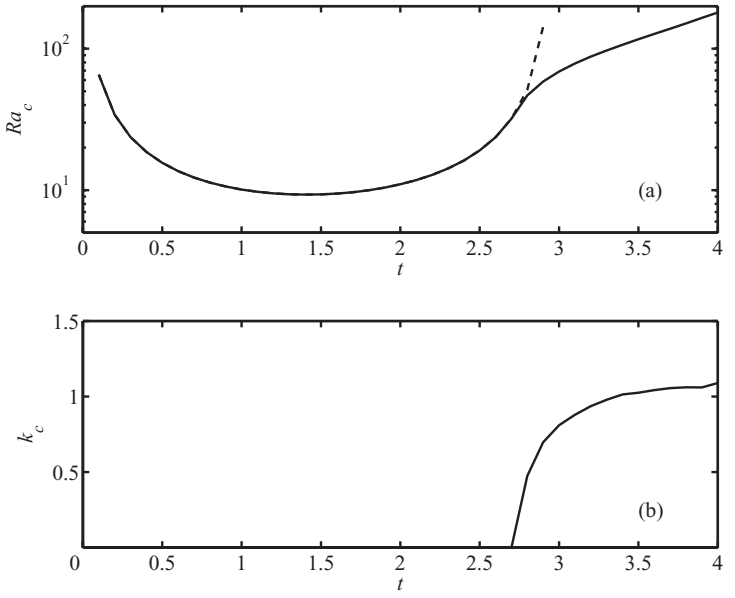

FIGURE 3. Numerical and asymptotic results for (a) Ra_c, and (b) k_c at $x = 3$. In (a) the dashed line is the asymptotic result (3.13).

4 Results and discussion

4.1 Introductory remarks

The results of this paper are divided into two sections. The first looks at the details of the stability problem, including how the stability of the water column evolves with time and the structure of the secondary circulation. The second considers the implications for the evolution of the thermal bar system.

4.2 The stability problem

Figure 3 shows typical results for the evolution of the critical Rayleigh number Ra_c and the critical wavenumber k_c at $x = 3$. Initially Ra_c is infinite as no heat has been added to the water column and hence there is no unstable density structure. As heat is added to the system, the water column becomes increasingly unstable, which is shown via the initially decreasing Ra_c in Figure 3(a). This decrease in Ra_c continues until the surface temperature reaches 1 (at $t \approx 1.2$) after which adding heat leads to a stable and thickening surface layer. As the thickness of this layer increases, Ra_c also increases. The transition from decreasing to increasing Ra_c occurs within the $k_c = 0$ regime, which means the asymptotic results of Section 3.2 capture this transition.

Some time later, once the stable layer has grown to encompass a significant fraction of the local depth, the $k \to 0$ results are no longer valid. The growth of the stable surface layer can be seen in Figure 2. For $x = 3$ this happens at $t \approx 2.7$ (see Figure 3(b)). This time also corresponds to the numerical and asymptotic calculations of Ra_c diverging in

https://doi.org/10.1017/S0956792512000344 Published online by Cambridge University Press

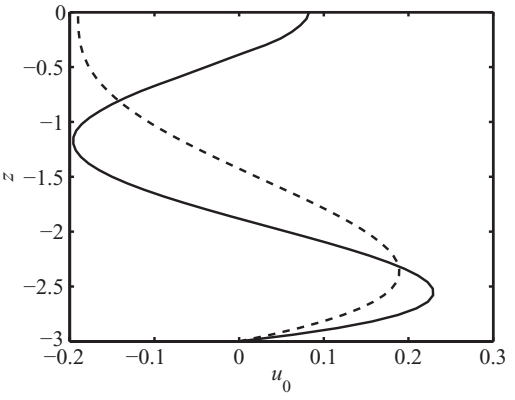

FIGURE 4. Two profiles of u_0 at $x = 3$ from the numerical calculations showing the transition from single cell ($t = 2$, dashed line) to double cell ($t = 3.5$, solid line).

Figure 3(a). For t slightly larger than this value, the asymptotic results have $Ra_c < 0$, which means that the water column is stable to perturbations with $k = 0$. Physically, the stable surface layer has isolated the unstable deeper layer from the insulated boundary condition at $z = 0$. Since it is the insulated boundary condition that leads to $k_c = 0$, the asymptotic results break down.

There is another significant transition that occurs in the stability problem. Figure 4 shows two profiles of u_0, the eigenfunction associated with the secondary motion. Note that at $t = 2$ the numerical profile shown in Figure 4 is indistinguishable (to graphical accuracy) from the asymptotic result given in (3.10). However, the profile at $t = 3.5$ is in a region where the $k \to 0$ results are not valid and the asymptotic result is not shown. The profile for $t = 2$ (dashed line) shows that the secondary motion consists of a single cell that encompasses the entire depth. The profile at $t = 3.5$ (solid line) has a double cell structure with a smaller and weaker cell sitting at the surface. This two-cell circulation structure was also seen in [20] where there was also a stable layer overlying an unstable layer. The interpretation in [20] was that the weaker upper cell was being driven by the viscous transfer of momentum from the deeper and stronger cell that was in turn driven by the unstable density structure. The transition from single to double cell circulation can be characterised by the surface velocity $u_0|_{z=0}$ being zero. This transition happens just before k_c becomes non-zero, so it is accurately captured by the asymptotic results.

Eventually, the water column will have a temperature greater than 1 over its entire depth (not shown in Figure 3). After this time the water column is stably stratified and adding more heat strengthens the stratification. Since the background temperature (2.18) attains its minimum at $z = -x$, the moment that $T^{(0)}|_{z=-x} = 1$ corresponds to $Ra_c = \infty$ and after this time the water column is stably stratified.

The above discussion has used the water column at $x = 3$ as an example. Other values of x have qualitatively similar behaviour. The main difference is the timing of the transitions from one regime to another. However, the transitions happen in the same order for all values of x.

https://doi.org/10.1017/S0956792512000344 Published online by Cambridge University Press

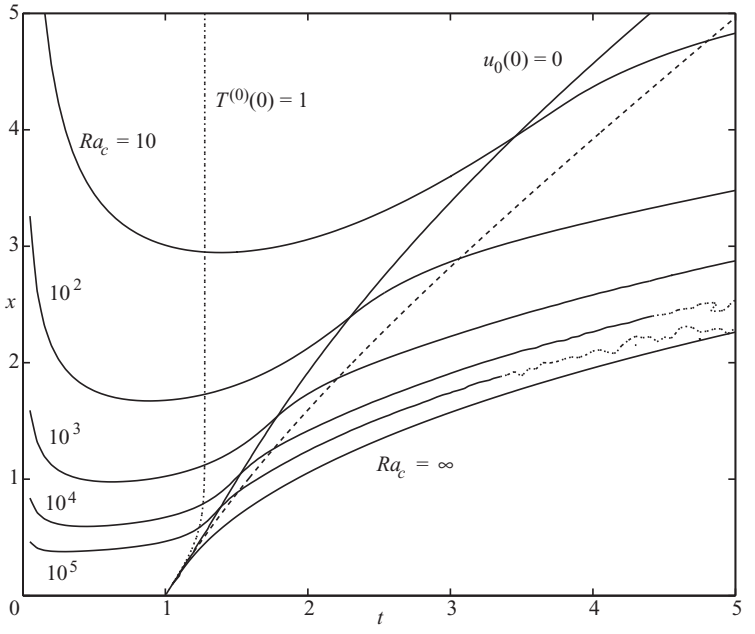

FIGURE 5. Contours of the numerically calculated Ra_c in the (t, x)-plane for $\eta = 1$ and $\sigma = 10$. The $Ra_c = \infty$ contour is determined by points where $T^{(0)}|_{z=-x} = 1$. Also shown is the location where the surface temperature $T^{(0)}|_{z=0} = 1$ (dotted line), the location where $u_0|_{z=0} = 0$ (solid line) and the location where the vertically averaged temperature is 1 (dashed line).

4.3 The thermal bar system

Figure 5 summarises the results of this paper. It shows contours in the (t, x)-plane of the numerically calculated Ra_c. It also includes the $Ra_c = \infty$ contour which corresponds to the points where $T^{(0)}|_{z=-x} = 1$. For points in the (t, x)-plane below this contour the water column is stably stratified over the entire depth. For points above this contour secondary motion can be expected if Ra exceeds the critical value associated with that point. Note that the numerically calculated contours become inaccurate near the $Ra_c = \infty$ contour (indicated by the dotted contours in Figure 5). This is because the numerical procedure is unable to accurately solve the stability problem when the thickness of the unstable layer at the base of the water column becomes very thin compared with the stable layer above it.

As noted above, the water column is initially stable and for small times Ra_c decreases as t increases. Deeper regions are less stable than the shallow regions where viscous effects are relatively greater. After some time (which is depth-dependent) Ra_c starts to increase indicating that the water column is becoming more stable. In the deeper parts of the domain this time corresponds closely to the time at which the surface temperature reaches 1 (indicated by the dotted line in Figure 5) and a stable surface layer starts to form. In the shallows where vertical diffusion of heat becomes important it happens sooner.

As time progresses the water column becomes more stable and the thickness of the stable surface layer increases. At some point (again, depth dependent) there is a transition

https://doi.org/10.1017/S0956792512000344 Published online by Cambridge University Press

from single-celled to double-celled secondary motion. After this time the turnover due to the instability does not occur over the entire depth. There is mixing at depth below the stably stratified surface layer within which there is a relatively weak circulation. For the thermal bar system this transition (indicated by the $u_0(0) = 0$ contour in Figure 5) marks the leading edge of the stably stratified surface layer. Note that in Figure 5 this transition happens before the vertically averaged temperature has reached 1 (shown as a dashed line in Figure 5). The dashed line is the analogue of (1.1) for the model of this paper. That is, the head of the stably stratified surface layer is further out from the shore than (1.1) would predict. This apparent greater than (1.1) propagation speed occurs despite there being no horizontal transport of heat in this model – it is entirely due to stability characteristics of the local water column.

Eventually the entire water column is stably stratified which marks the passing of the thermal bar and the establishment of summer conditions. In the model of this paper this corresponds to the temperature at the base of the water column reaching 1 which corresponds to the $Ra_c = \infty$ contour.

To summarise: For a fixed distance from the shore the passage of the thermal bar system is marked by a number of transitions. First the surface temperature reaches 1 which marks the establishment of a stable surface layer. This happens at more or less the same time for all depths with the exception being in the shallows where the water is shallower than the attenuation depth of the heating. Despite there being a stable surface layer, the water column is still unstable over its entire depth with the secondary motion consisting of a single cell encompassing the entire depth of the water column. The next transition is from single- to double-celled secondary motion. Here the water column does not turn over its entire depth. This means that the stable surface layer is not mixed with the deeper parts of the water column and in a lake this marks the establishment of a permanent surface layer. This happens before the vertically averaged temperature has reached 1, the traditional marker for the arrival of the thermal bar. The final transition to summer conditions is when the temperature of the entire water column becomes greater than 1 after which the present model predicts no secondary motion. The timings of these transitions depend on the local depth with the time between each transition increasing with depth. This latter point means that the horizontal extent of the thermal bar region increases as it moves away from the shore.

5 Concluding remarks

This paper has presented a framework for the evolution of the thermal bar system that is based on the instantaneous stability of the local water column. This framework leads to the thermal bar apparently moving out from the shore at a slightly greater speed than the vertically mixed model of Elliott and Elliott [9] despite there being no horizontal heat transfer in the model. The establishment of summer conditions is marked by a number of transitions as the stability characteristics of the warming water column evolve.

There are a number of obvious shortcomings with this model. Firstly, horizontal transport has been ignored which is unreasonable for lakes with bottom slopes larger than $\sim 10^{-2}$. All laboratory experiments of the thermal bar system have bottom slopes $\sim 10^{-1}$ so the present results are not applicable to experimental results at least for later

https://doi.org/10.1017/S0956792512000344 Published online by Cambridge University Press

times when significant horizontal currents have become established. Secondly, the stability problem is formulated using a pure conduction solution of the temperature structure which takes no account of any vertical mixing that might have previously occurred. Presumably any vertical mixing will tend to stabilise the water column which might lead to the thermal bar moving out more quickly than predicted by the model in this paper. Less significant shortcomings include the simplicity of the thermal forcing model.

Acknowledgements

The author would like to thank S. Brown and the anonymous reviewers for useful comments on earlier drafts of this paper.

References

[1] Chapman, C. J. & Proctor, M. R. E. (1980) Non-linear Rayleigh-Bénard convection between poorly conducting boundaries. *J. Fluid Mech.* **101**, 749–782.
[2] Coates, M. J. & Patterson, J. C. (1993) Unsteady natural-convection in a cavity with nonuniform absorption of radiation. *J. Fluid Mech.* **256**, 133–161.
[3] Coates, M. J. & Patterson, J. C. (1994) Numerical simulations of the natural-convection in a cavity with nonuniform internal sources. *Int. J. Heat Fluid Flow* **15**(3), 218–225.
[4] Cormack, D. E., Leal, L. G., & Imberger, J. (1974) Natural convection in a shallow cavity with differentially heated end walls. Part 1. asymptotic theory. *J. Fluid Mech.* **65**, 209–229.
[5] Csanady, G. T. (1971) On the equilibrium shape of the thermocline in a shore zone. *J. Phys. Oceanogr.* **1**, 263–270.
[6] Demchenko, N., Chubarenko, I. & van Heijst, G. (2012, April) On the fine structure of the thermal bar front. *Environ. Fluid Mech.* **12**(2), 161–183, 10.1007/s10652-011-9223-2.
[7] Drazin, P. G. & Ried, W. H. (2004) *Hydrodynamic Stability*, 2nd ed., Cambridge Texts in Appied Mathematics, Cambridge University Press, Cambridge, UK.
[8] Elliott, G. H. (1971) A mathematical study of the thermal bar. In: *Proceedings of the 14th Conference on Great Lakes Research*, University of Toronto, Ontario, Canada, April 19–21, Intl. Assoc. Great Lakes Res., pp. 545–554.
[9] Elliott, G. H. & Elliott, J. A. (1970) Laboratory studies on the thermal bar. In: *Proceedings of the 13th Conference on Great Lakes Research*, Intl. Assoc. Great Lakes Res., pp. 413–418.
[10] Farrow, D. E. (1995a) An asymptotic model for the hydrodynamics of the thermal bar. *J. Fluid Mech.* **289**, 129–140.
[11] Farrow, D. E. (1995b) A numerical model of the hydrodynamics of the thermal bar. *J. Fluid Mech.* **303**, 279–295.
[12] Farrow, D. E. (2002) A model of the thermal bar in the rotating frame including vertically non-uniform heating. *Environ. Fluid Mech.* **2**, 197–218.
[13] Farrow, D. E. & McDonald, N. R. (2002) Coriolis effects and the thermal bar. *J. Geophys. Res.* (Oceans) **107** (C5) doi:10.1029/2000JC000727.
[14] Farrow, D. E. & Patterson, J. C. (1994) The daytime circulation and temperature structure in a reservoir sidearm. *Int. J. Heat Mass Transfer* **37**(13), 1957–1968.
[15] Gresho, P. M. & Sani, R. L. (1971) The stability of a fluid layer subjected to a step change in temperature: Transient vs. frozen time analysis. *Int. J. Heat Mass Transfer* **14**, 207–221.
[16] Huang, J. C. K. (1972) The thermal bar. *Geophys. Fluid Dyn.* **3**, 1–28.
[17] Kreyman, K. D. (1989) Thermal bar based on laboratory experiments. *Oceanology* **29**(6), 695–697.
[18] Malm, J. (1995) Spring circulation associated with the thermal bar in large temperate lakes. *Nordic Hydrol.* **26**, 331–358.

[19] Malm, J., Mironov, D., Terzhevik, A. & Jönsson, L. (1994) Investigation of the sprint thermal regime in Lake Ladoga using field and satellite data. *Limnol. Oceanogr.* **39**(6), 1333–1348.

[20] Roberts, A. J. (1985) An analysis of near-marginal, mildly penetrative convection with heat flux prescribed on the boundaries. *J. Fluid Mech.* **158**, 71–93.

[21] Zilitinkevich, S. S., Kreiman, K. D. & Terzhivik, A. Yu. (1992) The thermal bar. *J. Fluid Mech.* **236**, 27–42.

[22] Zilitinkevich, S. S. & Malm, J. (1993) A theoretical model of thermal bar movement in a circular lake. *Nordic Hydrol.* **24**, 13–30.